**GPH-International Journal of Applied Science**
(Online ISSN 3050-9653)
Volume 07 | Issue 01 | January 2024
*Published by*: Global Publication House
*DOI:* https://doi.org/10.5281/zenodo.20374646
*Available online at:* www.gphjournal.org
*Journal homepage:* https://gphjournal.org/index.php/as/index

# Mathematical Analysis of a Fractional-Order Model of Zika Virus Transmission with Treatment Effects

**Ugo, D. C.[1], Okofu, M. B.[2], Amos J.[3], Ejikeme, C. L.*[2], Onoja K. A[4], Agbata, B. C.[5]**

[1]*Department of Mathematics, Faculty of Physical Sciences, University of Nigeria Nsukka, Nigeria.*
[2]*Department of Mathematics University of Nigeria, Nsukka, Nigeria.*
[3]*Department of Mathematical Sciences Prince Abubakar Audu University, Anyigba, Nigeria.*
[4]*Department of Pharmaceutical and Medicinal Chemistry, Faculty of Pharmaceutical Sciences, Nnamdi Azikiwe University, Awka, Nigeria.*
[5]*Department of Mathematics and Statistics, Faculty of Science, Confluence University of Science and Technology, Osara, Nigeria.*
*Corresponding author (Ejikeme Chioma) chioma.ejikeme@unn.edu.ng

## Abstract

Zika virus is a mosquito-borne viral infection primarily transmitted by *Aedes* species mosquitoes. It gained global attention due to its rapid spread and its association with neurological complications and congenital abnormalities. Understanding its transmission dynamics is essential for effective control and prevention. In this study, a deterministic compartmental model is developed to investigate the transmission dynamics of Zika virus infection, with particular focus on the roles of treatment and contact rates in disease spread. The model incorporates both human and vector populations and captures key processes such as infection, recovery, and reinfection. Numerical simulations are performed to examine how variations in treatment and contact rates influence the spread of the disease and the distribution of population compartments. The results indicate that higher contact rates lead to a substantial increase in new infections and cumulative case numbers, thereby intensifying transmission. In contrast, increased treatment rates reduce the number of infected individuals and overall disease burden while improving recovery levels within the human population. Further analysis of the basic reproduction number shows a nonlinear inverse relationship with treatment and contact parameters. Specifically, high contact rates combined with low treatment levels result in values of $R_0^Z$ greater than one, indicating sustained epidemic conditions. However, as treatment coverage increases, $R_0^Z$ decreases below unity, suggesting eventual disease elimination. The findings demonstrate that effective treatment strategies can mitigate the adverse effects of high contact rates by stabilizing the susceptible population and reducing infection peaks. This study highlights the importance of improving treatment access and reducing exposure through integrated control strategies as key approaches for controlling the spread of Zika virus infection.

## Keywords:

*Zika virus infection, Deterministic compartmental model, Stability analysis, Basic reproduction number, Numerical simulations.*

## Introduction

Zika virus (ZIKV) is a mosquito-borne flavivirus primarily transmitted by *Aedes aegypti* and *Aedes albopictus*, and has emerged as a significant global public health concern, particularly since the large outbreaks recorded between 2015 and 2016 in the Americas [3][4]. Although initially identified in 1947, the virus remained relatively understudied until its rapid spread across South and Central America highlighted its epidemic potential [3]. Early empirical studies documented widespread transmission in immunologically naïve populations, facilitated by urbanization, globalization, and favorable climatic conditions for vector proliferation [4][5]. The sudden increase in cases, particularly in Brazil, prompted urgent international attention and accelerated scientific research into its epidemiology, pathogenesis, and control strategies [6]. A major turning point in ZIKV research was the discovery of its association with severe neurological complications, especially congenital abnormalities. Several empirical studies established a strong causal link between maternal ZIKV infection and microcephaly in newborns [1][2][5]. Clinical and pathological investigations confirmed the presence of the virus in fetal brain tissues, providing direct evidence of vertical transmission and neurotropism [1]. Large cohort and observational studies further demonstrated increased risks of congenital Zika syndrome (CZS), which encompasses a range of developmental abnormalities beyond microcephaly, including vision impairment and cognitive deficits [6][8][9]. Additionally, research identified an association between ZIKV infection and Guillain–Barré syndrome in adults, further underscoring its neurological impact [7].

Beyond its clinical manifestations, ZIKV exhibits complex transmission dynamics that extend beyond traditional vector-borne pathways. While mosquito transmission remains the dominant route, empirical evidence has confirmed alternative modes, including sexual transmission, maternal–fetal transmission, and persistence in bodily fluids [8][9]. Advances in molecular diagnostics, such as reverse transcription loop-mediated isothermal amplification (RT-LAMP), have improved the detection of diverse ZIKV lineages across regions [15]. Furthermore, modeling and epidemiological studies have revealed the virus's capacity for rapid spread and persistence in tropical and subtropical environments, supported by the adaptability of multiple vector species [4][9]. These findings highlight the challenges in controlling ZIKV transmission and preventing future outbreaks.

Recent studies conducted between 2020 and 2024 have expanded understanding of the long-term outcomes of ZIKV infection and its continued circulation in endemic regions. Cohort and longitudinal studies have demonstrated that children exposed to ZIKV in utero may experience delayed neurodevelopment even in the absence of microcephaly at birth [10][11]. Additionally, emerging research in regions such as Nigeria and Southeast Asia indicates ongoing viral circulation, with seroprevalence and molecular surveillance studies confirming endemicity and periodic outbreaks [12][13][14]. These findings suggest that, despite a decline in large-scale epidemics, ZIKV remains a persistent public health threat requiring continuous monitoring. Despite substantial progress in research, several challenges remain in the prevention and control of ZIKV. There is currently no licensed vaccine or specific antiviral treatment, and public health responses continue to rely heavily on vector control and surveillance strategies [3][4]. Environmental factors such as climate change, increased urbanization, and global travel may facilitate the re-emergence and geographic expansion of the virus [12][14] [15][16]. Consequently, ongoing research efforts are focused on vaccine development, improved diagnostic tools, and integrated vector management approaches. Addressing these gaps is essential for mitigating the long-term health, social, and economic impacts of ZIKV, particularly among vulnerable populations such as pregnant women and infants [10][11][13].

Biswas et al [17] developed a deterministic mathematical model to analyze Zika virus transmission incorporating both mosquito-borne and sexual transmission pathways. The study included the effects of human awareness and vector control strategies. The researchers

established equilibrium points and demonstrated that the disease-free equilibrium remained stable when the basic reproduction number was less than one. Their sensitivity analysis highlighted that vector control and public awareness significantly reduced transmission rates, emphasizing the importance of combined intervention strategies in controlling outbreaks. Ibrahim and Dénes [19] formulated a compartmental model that incorporated sexual transmission, vertical transmission, and microcephaly risk associated with Zika infection. The model distinguished between asymptomatic and symptomatic individuals and included compartments for infants affected by microcephaly. The study demonstrated that vertical transmission played a critical role in sustaining infections and increasing disease burden. Their findings suggested that targeting pregnant women and reducing sexual transmission were essential components of effective control strategies. Murugappan et al [18] developed a mathematical model focusing on the transmission dynamics of Zika virus across different demographic groups, including males, females, and children. The study analyzed equilibrium and stability conditions to determine which populations were most affected. The results indicated that demographic heterogeneity significantly influenced disease spread, with certain groups contributing disproportionately to transmission. The model provided insights into targeted intervention strategies based on population structure. Wang et al [20] proposed a mathematical model that incorporated multiple transmission routes, including vector-borne, sexual, and vertical transmission, using data from Brazil. The study demonstrated that the coexistence of multiple transmission pathways significantly increased the complexity of controlling the disease. Their simulations showed that ignoring non-vector transmission routes could lead to underestimation of outbreak magnitude. The model emphasized the need for integrated intervention strategies addressing all transmission modes simultaneously. Zhu et al [21] investigated a stochastic optimal control model of Zika virus transmission using the Legendre spectral collocation method. The study incorporated randomness in transmission dynamics to better reflect real-world uncertainties. The results showed that optimal control strategies, including vector reduction and treatment interventions, significantly minimized infection levels when applied efficiently. The study contributed to advancing computational approaches in epidemiological modeling by integrating stochastic processes with optimal control theory.

The aim of this study is to develop a fractional mathematical model to investigate the dynamics of Zika virus transmission incorporating treatment as a control strategy. To achieve this aim, the following specific objectives are set out: (i) to formulate a mathematical model for Zika virus transmission that incorporates treatment intervention; (ii) to determine the disease-free equilibrium points of the model; (iii) to derive the basic reproduction number ($\Re_0$) of the model; (iv) to analyze the stability of the equilibrium points of the model; (v) to perform sensitivity analysis of the model parameters in order to identify those that significantly influence the transmission dynamics of Zika virus; (vi) to conduct numerical simulations of the developed model; and (vii) to solve the mathematical model using the Adams–Bashforth–Moulton method.

The novelty of this study lies in the development and analysis of a fractional-order mathematical model for Zika virus transmission that incorporates treatment as a control strategy, providing a more realistic representation of memory and hereditary effects in disease dynamics. Unlike classical integer-order models, the use of fractional calculus captures the complex biological and temporal behaviors associated with Zika virus spread more effectively. The study further derives the basic reproduction number ($\Re_0$) and investigates both the disease-free equilibrium and its stability within a fractional framework, which is less explored in existing literature. In addition, a comprehensive sensitivity analysis is conducted to identify key parameters influencing transmission dynamics, thereby offering insights for effective intervention strategies. The model is also numerically simulated using the Adams–Bashforth–Moulton method, enabling accurate approximation of the fractional system and enhancing the robustness of the analytical results.

## Model Formulation

In formulating a mathematical model of Zika virus infectious disease, the population is sub-divided into eight compartments such as: Susceptible human population $(S_h)$, Exposed individuals $(\mathrm{E}_Z)$, Zika virus infected individuals $(\mathrm{I}_Z)$ individuals on Zika virus treatment $(\mathrm{T}_Z)$, Recovered human population from Zika virus $(R_Z)$, susceptible vectors $(S_V)$, Exposed vectors $(\mathrm{E}_V)$, and infected vectors $(I_V)$. The susceptible humans are recruited at the rate of $\Lambda_h$, The effective contact rate between the susceptible and infected humans, susceptible individuals and humans on Zika virus treatment, susceptible vectors and infected humans, susceptible vectors and infected humans, susceptible individuals and infected vectors are $\beta_1, \beta_2, \beta_V, \beta_3$ respectively. Human progresses from exposed Zika virus classes to infected class at the rate $\alpha$, and receive treatment at the rate of $\theta$, humans recovered due to treatment at the rate of $\sigma$, human population and vector population die naturally at the rate of $\mu_h, \mu_V$ respectively. Human population die due to disease at the rate of $\delta_1, \delta_2, \delta_V$ respectively. Exposed Vector population progresses to infected vector population at the rate of $\theta_V$ The recovered human population become susceptible again after sometimes at the rate of $\omega$ It is assumed that humans who have recovered from the Zika virus can lose their immunity over time and become susceptible to reinfection. We assumed that infection with the Zika virus can lead to death in some individuals within the human population. Additionally, the model considered that natural death occurs within the human population regardless of disease status. Furthermore, it assumes that the transmission of the Zika virus occurs through interactions between susceptible and infected individuals. Finally, the model assumed that recovery from the infection does not guarantee lifelong immunity, thereby allowing the possibility of repeated cycles of infection within the population.

## Model Flow Diagram

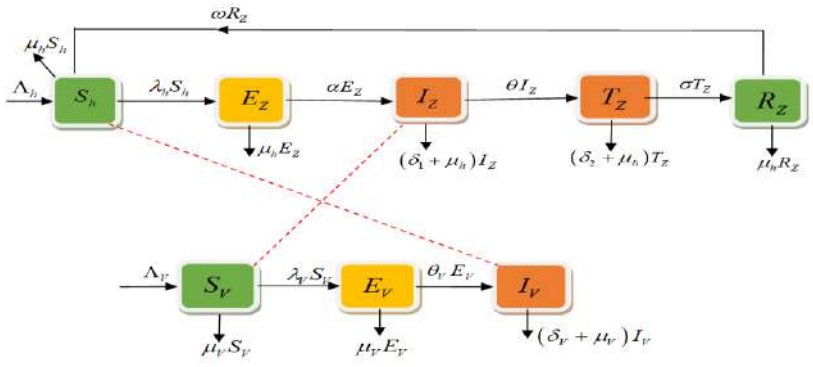


Figure 1. Zika virus model flow Diagram

**Model Equations**

$$\frac{dS_h}{dt} = \Lambda_h + \omega R_Z - \lambda_h S_h - \mu_h S_h,$$

$$\frac{dE_Z}{dt} = \lambda_h S_h - (\alpha + \mu_h) E_Z,$$

$$\frac{dI_Z}{dt} = \alpha E_Z - (\theta + \delta_1 + \mu_h) I_Z, \qquad (1)$$

$$\frac{dT_Z}{dt} = \theta I_Z - (\sigma + \delta_2 + \mu_h) T_Z,$$

$$\frac{R_Z}{dt} = \sigma T_Z - (\omega + \mu_h) R_Z,$$

$$\frac{dS_V}{dt} = \Lambda_V - \lambda_V S_V - \mu_V S_V,$$

$$\frac{dE_V}{dt} = \lambda_V S_V - (\theta_V + \mu_V) E_V,$$

$$\frac{dI_V}{dt} = \theta_V E_V - (\delta_V + \mu_V) I_V.$$

Where $\lambda_h = \frac{(\beta_1 I_Z + \beta_2 T_Z + \beta_3 I_V)}{N_h}$ and $\lambda_V = \frac{\beta_V I_Z}{N_h}$.

**Table 1: Model Variables and Parameters Descriptions**

| **Variables** | **Descriptions** |
|---|---|
| $S_h$ | Susceptible human population to Zika virus |
| $E_Z$ | Exposed human population to Zika virus |
| $I_Z$ | Infected human with Zika virus |
| $T_Z$ | Human population on Zika virus treatment |
| $R_Z$ | Recovered human population from Zika virus |
| $S_V$ | Susceptible vector population |
| $E_V$ | Exposed vector population |
| $I_V$ | Infected vector population |
| **Parameters** | **Descriptions** |
| $\Lambda_h$ | Recruitment rate of Susceptible human population to Zika virus |

| | |
|---|---|
| $\beta_1$ | Contact rate between the susceptible humans and infected human with Zika virus |
| $\beta_2$ | Contact rate between the susceptible humans and individuals on Zika virus treatment |
| $\beta_3$ | Contact rate between the susceptible humans and vector population |
| $\alpha$ | Progression rates from exposed humans to Zika virus class to infected human with Zika virus population |
| $\theta$ | Treatment rate of infected humans |
| $\theta_V$ | Progression rate of vector population. |
| $\beta_V$ | Contact rate between the infected humans and susceptible vectors |
| $\mu_h$ | Natural death rate of human population |
| $\mu_V$ | Natural death rate of vector population |
| $\delta_1$ | Disease induced death rate of infected humans with Zika virus |
| $\delta_2$ | Disease induced death rate of humans on Zika virus treatment |
| $\delta_V$ | Death induced due to an attempt to bite humans |
| $\Lambda_V$ | Recruitment rate of vectors |
| $\mu_V$ | Natural death rate of vectors |
| $\omega$ | Rate at which recovered humans become susceptible again |
| $\sigma$ | Recovery due to treatment rate |

**Preliminaries**

Definition 1: Let $f \in \Lambda^{\infty}(R)$ then the left and right Caputo fractional derivative of the function $f$ is given by

$$ {}^{C}D_t^{\psi} f(t) = \left( t^{0}D_t^{-(\psi-\psi)} \left( \frac{d}{dt} \right)^{\psi} f(t) \right) $$

$$ {}^{C}D_t^{\psi} f(t) = \frac{1}{\Gamma(n-\psi)} \int_0^t \left( (t-\lambda)^{\psi-\psi-1} f^n(\lambda) \right) d\lambda \qquad (2) $$

The same way

$$ {}^{C}D_t^{\psi} f(t) = \left( D_T^{-(\psi-\psi)} \left( \frac{-d}{dt} \right)^{\psi} \right) f(t) $$

$$ {}^{C}D_T^{\psi} f(t) = \frac{(-1)^n}{\Gamma(n-\psi)} \int_t^T (\lambda - t)^{n-\psi-1} f^n(\lambda) d\lambda $$

Definition 2: The generalized Mittag-Leffler function $E_{\gamma,\beta}(x)$ for $x \in R$ is given by

$$E_{\gamma,\beta}(x)=\sum_{n=0}^{\infty}\frac{x^n}{\Gamma(\gamma n+\omega)},\ \gamma,\omega>0 \tag{3}$$

which can also be represented as

$$E_{\gamma,\psi}(x)=xE_{\gamma,\gamma+\psi(x)}+\frac{1}{\Gamma(\psi)} \tag{4}$$

$$E_{\gamma,\omega}(x)=L\left[t^{\omega-1}E_{\gamma,\omega(\pm\omega t^{\eta})}\right]=\frac{S^{\gamma-\psi}}{S^{\gamma}\pm\omega}. \tag{5}$$

Proposition 1.1

Let $f\in\Lambda^{\infty}(R)\cap C(R)$ and $\psi\in R, n-1<\psi<n,$

therefore, the conditions given below holds:

1. ${}_{t_0}^{C}D_t^{\psi}I^{\psi}f(t)=f(t)$

2. ${}_{t_0}^{C}D_t^{\psi}I^{\psi}f(t)=f(t)-\sum_{k-0}^{n-k}\frac{t^k}{K!}f^k(t_0)$

## Fractional Zika Virus Mathematical Model

In this section, we reformulate the integer-order Zika virus model presented in Equation (1) by incorporating the Caputo fractional derivative operator [23,24,25]. This modified model provides greater flexibility than the classical model in equation (1), as the fractional-order framework allows the system's output to be tuned to exhibit a wider range of dynamic behaviors. Accordingly, the fractional Zika virus model is expressed as follows:

$$\begin{aligned}
{}^{C}D_t^{\psi}S_h&=\Lambda_h+\omega R_Z-\frac{(\beta_1 I_Z+\beta_2 T_Z+\beta_3 I_V)}{N_h}S_h-\mu_h S_h,\\
{}^{C}D_t^{\psi}E_Z&=\frac{(\beta_1 I_Z+\beta_2 T_Z+\beta_3 I_V)}{N_h}S_h-(\alpha+\mu_h)E_Z,\\
{}^{C}D_t^{\psi}I_Z&=\alpha E_Z-(\theta+\delta_1+\mu_h)I_Z,\\
{}^{C}D_t^{\psi}T_Z&=\theta I_Z-(\sigma+\delta_2+\mu_h)T_Z,\\
{}^{C}D_t^{\psi}R_Z&=\sigma T_Z-(\omega+\mu_h)R_Z,\\
{}^{C}D_t^{\psi}S_V&=\Lambda_V-\frac{\beta_V I_Z}{N_h}S_V-\mu_V S_V,
\end{aligned} \tag{6}$$

$${}^{C}D_t^{\psi} E_V = \lambda_V S_V - \left(\theta_V + \mu_V\right) E_V,$$

$${}^{C}D_t^{\psi} I_V = \theta_V E_V - \left(\delta_V + \mu_V\right) I_V.$$

Subject to positive initial conditions

$$S_h\left(0\right) = S_{h0},\ \mathrm{E}_Z\left(0\right) = E_{Z0}, \mathrm{I}_Z\left(0\right) = I_{Z0}, T_Z\left(0\right) = T_{Z0},$$
$$R_Z\left(0\right) = R_{Z0}, \mathrm{S}_V\left(0\right) = \mathrm{S}_{V0}, \mathrm{E}_V\left(0\right) = E_{V0}, \mathrm{I}_V\left(0\right) = I_{V0}\ . \tag{7}$$

We considered the non-negativity of the initial values

$$N_h(t) \le \frac{\Lambda_h}{\mu_h} \quad \text{as} \quad t \to \infty$$

Secondly, if $\limsup N_{h0}(t) \le \frac{\Lambda_h}{\mu_h}$, then our model feasible domain is given by:

$$\Omega_h = \left\{\left(S_h,\ \mathrm{E}_Z, \mathrm{I}_Z, T_Z, R_Z, \mathrm{S}_V, \mathrm{E}_V, \mathrm{I}_V\right) \subset R_+^8 : \left(S_h + \mathrm{E}_Z + \mathrm{I}_Z + T_Z + R_Z\right) \le \frac{\Lambda_h}{\mu_h}\right\}, \text{so that,}$$

$$\Omega = \Omega_h \times \Omega_V \subset R_+^8,$$

hence $\Omega$ is positively invariant.

If $\left(S_{h0},\ \mathrm{E}_{Z0}, \mathrm{I}_{Z0}, T_{Z0}, R_{Z0}, \mathrm{S}_V, \mathrm{E}_V, \mathrm{I}_V\right)$ are non-negative, then the solution of model (6) will be non-negative for $t > 0$. From Eq. (4.5), selecting the first equation, we obtained:

$${}^{C}D_t^{\psi} S_h = \Lambda_h + \omega R_Z - \frac{\left(\beta_1 I_Z + \beta_2 T_Z + \beta_3 I_V\right)}{N_h} S_h - \mu_h S_h,$$

$${}^{C}D_t^{\psi} S_h + \frac{\left(\beta_1 I_Z + \beta_2 T_Z + \beta_3 I_V + \mu_h\right)}{N_h} S_h + = \Lambda_h$$

But $\Lambda_h \ge 0$, then

$${}^{C}D_t^{\eta} S_h + \left(\lambda_h + \mu_h\right) S_h \ge 0.$$

Applying the Laplace transform we obtained:

$$L\left[{}^{C}D_t^{\psi} S_h\right] + L\left[\frac{\left(\beta_1 I_Z + \beta_2 T_Z + \beta_3 I_V + \mu_h\right)}{N_h} S_h\right] \ge 0$$

$$S_h^{\psi} S_h\left(s_h\right) - S_h^{\psi-1} S_h\left(0\right) + \left(\lambda_h + \mu_h\right) S_h\left(s\right) \ge 0,$$

$$S_h(s) \geq \frac{S_h^{\psi-1}}{S_h^{\psi}+(\lambda_h+\mu_h)} S_h(0). \tag{8}$$

By taking the inverse Laplace transform, we obtained:

$$S_h(t) \geq E_{t\psi,1}\left(-(\lambda_h+\mu_h)t^{\psi}\right)\mathrm{S}_{h0}. \tag{9}$$

Now since the term on the right-hand side of Eq. (9) is positive, we conclude that $S_h \geq 0$ for $t \geq 0$ . In the same way, we also have that $\left(\mathrm{E}_Z \geq 0, I_Z \geq 0, \mathrm{T}_Z \geq 0, \mathrm{R}_Z \geq 0, \mathrm{S}_V \geq 0, \mathrm{E}_V \geq 0, \mathrm{I}_V \geq 0\right)$. that is positives; therefore, the solution will remain in $R_+^8$ for all $t \geq 0$ with positive initial conditions [24,25].

**Boundedness of fractional model Equation**

The total human population from our model is given by:

$$N_h(t) = S_h(t) + E_Z(t) + I_Z(t) + T_Z(t) + \mathrm{R}_Z.$$

So from our fractional model (4.5), we now obtain:

$${}^{C}D_t^{\psi} N_h(t) = {}^{C}D_t^{\psi} S_h(t) + {}^{C}D_t^{\psi} E_Z(t) + {}^{C}D_t^{\psi} I_Z(t) + {}^{C}D_t^{\psi} T_Z(t) + {}^{C}D_t^{\psi}\,\mathrm{R}_Z.$$

$${}^{C}D_t^{\psi} N_h(t) = \Lambda_h - \mu_h N_h(t) \tag{10}$$

Taking the Laplace transformation of (10) we obtained:

$$L\left[{}^{C}D_t^{\psi} N_h(t)\right] = L\left[\Lambda_h - \mu_h N_h(t)\right]$$

$$S_h^{\psi} N_h(\mathrm{s}) - S_h^{\psi-1} N_h(0) + \mu_h N_h(s) \leq \frac{\Lambda_h}{\mu_h},$$

$$N_h(\mathrm{s}) \leq \frac{S_h^{\psi-1}}{\left(S^{\psi}+\mu_h\right)} N_h(0) + \frac{\Lambda_h}{S_h\left(S_h^{\psi}+\mu_h\right)} \tag{11}$$

Taking the inverse Laplace transform of Eq. (11) we have;

$$N_h(\mathrm{t}) \leq E_{h\psi,1}\left(\mu_h t^{\psi}\right) N_h(0) + \Lambda_h E_{h\psi,\psi+1}\left(\mu_h t^{\psi}\right) \tag{12}$$

At $t \to \infty$, the limit of Eq. (12) becomes:

$$\lim_{t\to\infty} Sup N_h(t) = \frac{\Lambda_h}{\mu_h}.$$

This means that, if $N_{h0} \le \frac{\Lambda_h}{\mu_h}$.

then $N_h(t) \le \frac{\Lambda_h}{\mu_h}$ which implies that, $N_h(t)$ is bounded.

Therefore, this region $\Omega = \Omega_h$, is well posed and equally feasible epidemiologically.

Similarly, the total Vector population from our model is given by;

$$N_V(t) = S_V(t) + E_V(t) + I_V(t).$$

So from our fractional model (6), we now obtain:

$${}^{C}D_t^{\psi} N_V(t) = {}^{C}D_t^{\psi} S_V(t) + {}^{C}D_t^{\psi} E_V(t) + {}^{C}D_t^{\psi} I_V(t).$$

$${}^{C}D_t^{\psi} N_V(t) = \Lambda_V - \mu_V N_V(t) \tag{13}$$

Taking the Laplace transformation of (13) we obtained:

$$L\left[{}^{C}D_t^{\psi} N_V(t)\right] = L\left[\Lambda_V - \mu_V N_V(t)\right],$$

$$S_V^{\psi} N_V(\mathrm{s}) - S_V^{\psi-1} N_V(0) + \mu_V N_V(s) \le \frac{\Lambda_V}{\mu_V},$$

$$N_V(\mathrm{s}) \le \frac{S_V^{\psi-1}}{\left(S^{\psi} + \mu_V\right)} N_V(0) + \frac{\Lambda_V}{S_V\left(S_V^{\psi} + \mu_V\right)}, \tag{14}$$

Taking the inverse Laplace transform of Eq. (14) we have;

$$N_V(\mathrm{t}) \le E_{V\psi,1}\left(\mu_V t^{\psi}\right) N_V(0) + \Lambda_V E_{V\psi,\psi+1}\left(\mu_V t^{\psi}\right) \tag{15}$$

At $t \to \infty$, the limit of Eq. (15) becomes:

$$\lim_{t\to\infty} Sup N_V(t) = \frac{\Lambda_V}{\mu_V}.$$

This means that, if $N_{V0} \le \frac{\Lambda_V}{\mu_V}$.

then $N_V(t) \le \frac{\Lambda_V}{\mu_V}$ which implies that, $N_V(t)$ is bounded.

We now conclude that, this region $\Omega = \Omega_V$ , is well posed and equally feasible epidemiologically.

### 4.4 Existence and Uniqueness of our Model Solution

Let the real non-negative be $H$ we consider $P = [0, \mathrm{J}]$.

All continuous function that exist on P belongs to $N_{he}^{0}(J)$ with norm as;

$$\|K\| = Sup\left\{\left|K(t)\right|, \mathrm{t} \in J\right\}.$$

The modeled system (6) along with specified initial (8) enables solving for a system of differential equations presented in (14).

$$\begin{aligned} {}^{c}D_{t}^{\psi} K(t) &= Z\left(t, \mathrm{K}(t)\right), 0 < t < J < \infty, \\ K(0) &= K_0. \end{aligned} \tag{16}$$

Where $K(t) = (S_h, \mathrm{E}_Z, \mathrm{I}_Z, T_Z, R_Z, \mathrm{S}_V, \mathrm{E}_V, \mathrm{I}_V)$. represents the classes and Z be a continuous function defined as follows;

$$Z\left(t, \mathrm{K}(t)\right) = \begin{pmatrix} Z_1\left(t, S_h(t)\right) \\ Z_2\left(t, \mathrm{E}_Z(t)\right) \\ Z_3\left(t, \mathrm{I}_Z(t)\right) \\ Z_4\left(t, \mathrm{T}_Z(t)\right) \\ Z_5\left(t, \mathrm{R}_Z(t)\right) \\ Z_6\left(t, \mathrm{S}_V(t)\right) \\ Z_7\left(t, \mathrm{E}_V(t)\right) \\ Z_8\left(t, \mathrm{I}_V(t)\right) \end{pmatrix} = \begin{pmatrix} \Lambda_h + \omega R_Z - \dfrac{(\beta_1 I_Z + \beta_2 T_Z + \beta_3 I_V)}{N_h} S_h - \mu_h S_h \\ \dfrac{(\beta_1 I_Z + \beta_2 T_Z + \beta_3 I_V)}{N_h} S_h - (\alpha + \mu_h) E_Z \\ \alpha E_Z - (\theta + \delta_1 + \mu_h) I_Z \\ \theta I_Z - (\sigma + \delta_2 + \mu_h) T_Z \\ \sigma T_Z - (\omega + \mu_h) R_Z \\ \Lambda_V - \dfrac{\beta_V I_Z}{N_h} S_V - \mu_V S_V \\ \dfrac{\beta_V I_Z}{N_h} S_V - (\theta_V + \mu_V) E_V \\ \theta_V E_V - (\delta_V + \mu_V) I_V \end{pmatrix}, \tag{17}$$

Using proposition (1.1), we have that,

$$S_h(t) = S_{h0} + I_t^{\psi}\left[\Lambda_h + \omega R_Z - \frac{(\beta_1 I_Z + \beta_2 T_Z + \beta_3 I_V)}{N_h} S_h - \mu_h S_h\right],$$

$$E_Z(t) = E_{Z0} + I_t^{\psi}\left[\frac{(\beta_1 I_Z + \beta_2 T_Z + \beta_3 I_V)}{N_h} S_h - (\alpha + \mu_h) E_Z\right],$$

(18)

$$I_Z(t) = I_{Z0} + I_t^{\psi}\left[\alpha E_Z - (\theta + \delta_1 + \mu_h) I_Z\right],$$

$$T_Z(t) = T_{Z0} + I_t^{\psi}\left[\theta I_Z - (\sigma + \delta_2 + \mu_h) T_Z\right],$$

$$R_Z(t) = R_{Z0} + I_t^{\psi}\left[\sigma T_Z - (\omega + \mu_h) R_Z\right],$$

$$S_V(t) = S_{V0} + I_t^{\psi}\left[\Lambda_V - \frac{\beta_V I_Z}{N_h} S_V - \mu_V S_V\right],$$

$$E_V(t) = E_{V0} + I_t^{\psi}\left[\frac{\beta_V I_Z}{N_h} S_V - (\theta_V + \mu_V) E_V\right],$$

$$I_V(t) = I_{V0} + I_t^{\psi}\left[\theta_V E_V - (\delta_V + \mu_V) I_V\right].$$

We obtain the Picard iteration of (18) as follows:

$$S_h(t) = S_{h0} + \frac{1}{\Gamma(\psi)}\int_0^t (t-\lambda_h)^{\psi-1} Z_1\left(\lambda_h, S_{h(n-1)}(\lambda_h)\right) \mathrm{d}\lambda_h,$$

$$E_Z(t) = E_{Z0} + \frac{1}{\Gamma(\psi)}\int_0^t (t-\lambda_h)^{\psi-1} Z_2\left(\lambda_h, \mathrm{E}_{\mathrm{Z}(n-1)}(\lambda_h)\right) \mathrm{d}\lambda_h, \tag{19}$$

$$I_Z(t) = I_{Z0} + \frac{1}{\Gamma(\psi)}\int_0^t (t-\lambda_h)^{\psi-1} Z_3\left(\lambda_h, \mathrm{I}_{\mathrm{Z}(n-1)}(\lambda_h)\right) \mathrm{d}\lambda_h,$$

$$T_Z(t) = T_{Z0} + \frac{1}{\Gamma(\psi)}\int_0^t (t-\lambda_h)^{\psi-1} Z_4\left(\lambda_h, \mathrm{T}_{\mathrm{Z}(n-1)}(\lambda_h)\right) \mathrm{d}\lambda_h,$$

$$R_Z(t) = R_{Z0} + \frac{1}{\Gamma(\psi)}\int_0^t (t-\lambda_h)^{\psi-1} Z_5\left(\lambda_h, \mathrm{R}_{\mathrm{Z}(n-1)}(\lambda_h)\right) \mathrm{d}\lambda_h,$$

$$S_V(t) = S_{V0} + \frac{1}{\Gamma(\psi)}\int_0^t (t-\lambda_h)^{\psi-1} Z_6\left(\lambda_h, \mathrm{S}_{\mathrm{V}(n-1)}(\lambda_h)\right) \mathrm{d}\lambda_h,$$

$$E_V(t) = E_{V0} + \frac{1}{\Gamma(\psi)}\int_0^t (t-\lambda_h)^{\psi-1} Z_7\left(\lambda_h, \mathrm{E}_{\mathrm{V}(n-1)}(\lambda_h)\right) \mathrm{d}\lambda_h,$$

$$I_V(t) = I_{V0} + \frac{1}{\Gamma(\psi)}\int_0^t (t-\lambda_h)^{\psi-1} Z_8\left(\lambda_h, \mathrm{I}_{\mathrm{V}(n-1)}(\lambda_h)\right)\mathrm{d}\lambda_h.$$

Transforming equation eq. (15) to get:

$$A(t) = A(0) + \frac{1}{\Gamma(\psi)}\int_0^t (t-\lambda_h)^{\psi-1} Z\left(\lambda_h, \mathrm{A}(\lambda_h)\right)\mathrm{d}\lambda_h. \tag{19}$$

**Lemma 1**, The equation (17) gives us the definition of the Lipchitz condition which vector satisfies; $Z\left(\mathrm{t}, \mathrm{K}(t)\right)$ on a set $[0, \mathrm{J}]\times R_+^8$ with the Lipchitz constant given as;

$$\beta = \max\begin{pmatrix}\left(\beta_1^* + \beta_2^* + \beta_3^* + \mu_h\right), (\alpha+\mu_h), (\theta+\delta_1+\mu_h), (\sigma+\delta_2+\mu_h)\\ , (\omega+\mu_h), (\mu_V), (\theta_V+\mu_V), (\delta_V+\mu_V)\end{pmatrix}.$$

Proof:

$$\left\|Z_1(t, S_h) - Z_1(t, S_{h1})\right\|,$$

$$= \left\|\Lambda_h + \omega R_Z - \frac{(\beta_1 I_Z + \beta_2 T_Z + \beta_3 I_V)}{N_h} S_h - \mu_h S_h - \Lambda_h + \omega R_Z - \frac{(\beta_1 I_Z + \beta_2 T_Z + \beta_3 I_V + \mu_h)}{N_h} - S_{h1}\right\|,$$

$$= \left\|-\Lambda_h + \omega R_Z - \frac{(\beta_1 I_Z + \beta_2 T_Z + \beta_3 I_{Vh})}{N_h}(S_h - S_{h1}) + \mu_h(S_h - S_{h1})\right\| \le \left(\beta_1^* + \beta_2^* + \beta_3^* + \mu_h\right)\|S_h - S_{h1}\| + \mu_h\|S_h - S_{h1}\|,$$

$$\therefore \left\|Z_1(t, S_h) - Z_1(t, S_{h1})\right\| \le \left(\beta_1^* + \beta_2^* + \beta_3^* + \mu_h\right)\|S_h - S_{h1}\|.$$

Similarly, we obtained the following:

$$\begin{aligned}
&\left\|Z_2(t, \mathrm{E}_Z) - Z_2(t, \mathrm{E}_{Z1})\right\| \le (\alpha+\mu_h)\|\mathrm{E}_Z - \mathrm{E}_{Z1}\|,\\
&\left\|Z_3(t, \mathrm{I}_Z) - Z_3(t, \mathrm{I}_{Z1})\right\| \le (\theta+\delta_1+\mu_h)\|I_Z - I_{Z1}\|,\\
&\left\|Z_4(t, \mathrm{T}_Z) - Z_4(t, \mathrm{T}_{Z1})\right\| \le (\sigma+\delta_2+\mu_h)\|T_Z - T_{Z1}\|,\\
&\left\|Z_5(t, \mathrm{R}_Z) - Z_5(t, \mathrm{R}_{Z1})\right\| \le (\omega+\mu_h)\|R_Z - R_{Z1}\|,\\
&\left\|Z_6(t, \mathrm{S}_V) - Z_6(t, \mathrm{S}_{V1})\right\| \le (\mu_V)\|\mathrm{S}_V - \mathrm{S}_{V1}\|,\\
&\left\|Z_7(t, \mathrm{E}_V) - Z_7(t, \mathrm{E}_{V1})\right\| \le (\theta_V+\mu_V)\|E_V - E_{V1}\|,\\
&\left\|Z_8(t, \mathrm{I}_V) - Z_8(t, \mathrm{I}_{V1})\right\| \le (\delta_V+\mu_V)\|I_V - I_{V1}\|.
\end{aligned} \tag{20}$$

Where we obtained:

$$\left\| Z\left(t, \mathrm{K}_1(t)\right) - Z\left(t, \mathrm{K}_2(t)\right) \right\| \le \psi \left\| K_1 - K_2 \right\|,$$

$$\beta = \max \begin{pmatrix} \left(\beta_1^* + \beta_2^* + \beta_3^* + \mu_h\right), \left(\alpha + \mu_h\right), \left(\theta + \delta_1 + \mu_h\right), \left(\sigma + \delta_2 + \mu_h\right) \\ , \left(\omega + \mu_h\right), \left(\mu_V\right), \left(\theta_V + \mu_V\right), \left(\delta_V + \mu_V\right) \end{pmatrix}. \quad (21)$$

**Lemma 2.** The initial value problem (6), (7) in Eq. (21) exists and will have a unique solution

$$K(t) \in D_c^0(E).$$

Applying PicardLindelöfand fixed-point conjecture, we consider the solution of

$$K(t) = S_h\left(K(t)\right),$$

where S is defined as the Picard operator expressed as ;

$$S_h : \mathrm{D}_c^0\left(\mathrm{E}, R_+^8\right) \to D_c^0\left(\mathrm{E}, R_+^8\right).$$

Therefore, (

$$S_h\left(K(t)\right) = K(0) + \frac{1}{\Gamma(\psi)} \int_0^t (t - \lambda_h)^{\psi - 1} Z\left(\lambda_h, \mathrm{K}(\lambda_h)\right) \mathrm{d}\lambda_h.$$

which becomes,

$$\left\| S_h\left(K_1(t)\right) - S_h\left(K_2(t)\right) \right\|$$

$$= \left\| \frac{1}{\Gamma(\psi)} \left[ \int_0^t (t - \lambda_h)^{\psi - 1} Z\left(\lambda_h, \mathrm{K}_1(\lambda_h)\right) - Z\left(\lambda_h, \mathrm{K}_2(\lambda_h)\right) \mathrm{d}\lambda_h \right] \right\|$$

$$\le \frac{1}{\Gamma(\psi)} \int_0^t (t - \lambda_h)^{\psi - 1} \left\| Z\left(\lambda_h, \mathrm{K}_1(\lambda_h)\right) - Z\left(\lambda_h, \mathrm{K}_2(\lambda_h)\right) \mathrm{d}\lambda_h \right\|.$$

$$\le \frac{\beta}{\Gamma(\psi)} \int_0^t (t - \lambda_h)^{\psi - 1} \left\| K_1 - K_2 \right\| d\lambda_h.$$

$$\left\| S_h\left(K_1(t)\right) - S_h\left(K_2(t)\right) \right\| \le \frac{\beta}{\Gamma(\psi + 1) S_h}. \quad (22)$$

When $\frac{\beta}{\Gamma(\psi + 1)} S_h \le 1,$

then the Picard operator gives a contradiction, so Eq.(6), (7) solution is unique [23,24].

**Lemma 3:** The initial value problem (6), (7) in Eq. (21) exists and will have a unique solution.

$$\mathrm{X}(t) \in A_c^0(f).$$

Using Picard-Lindelöf and fixed- point theory, we consider the solution of

$$A(t) = S_h\left(A(t)\right),$$

where S is defined as the Picard operator expressed as;

$$S_h : A_c^0\left(f, R_+^8\right) \to A_c^0\left(f, R_+^8\right).$$

Therefore,

$$S_h\left(A(t)\right) = A(0) + \frac{1}{\Gamma(\psi)}\int_0^t (t-\lambda_h)^{\psi-1} Z\left(\lambda_h, \mathrm{A}(\lambda_h)\right) \mathrm{d}\lambda_h.$$

This becomes,

$$\left\|S_h\left(A_1(t)\right) - S_h\left(A_2(t)\right)\right\|$$

$$= \left\| \frac{1}{\Gamma(\psi)}\left[\int_0^t (t-\lambda_h)^{\psi-1} Z\left(\lambda_h, \mathrm{A}_1(\lambda_h)\right) - Z\left(\lambda_h, \mathrm{A}_2(\lambda_h)\right) \mathrm{d}\lambda_h\right]\right\|,$$

$$\leq \frac{1}{\Gamma(\psi)}\int_0^t (t-\lambda_h)^{\psi-1} \left\| Z\left(\lambda_h, \mathrm{A}_1(\lambda_h)\right) - Z\left(\lambda_h, \mathrm{A}_2(\lambda_h)\right) \mathrm{d}\lambda_h \right\|.$$

$$\leq \frac{\beta}{\Gamma(\psi)}\int_0^t (t-\lambda_h)^{\psi-1} \left\| A_1 - A_2 \right\| d\lambda_h.$$

$$\left\|S_h\left(A_1(t)\right) - S_h\left(A_2(t)\right)\right\| \leq \frac{\beta}{\Gamma(\psi+1) S_h}. \tag{23}$$

When $\frac{\beta}{\Gamma(\psi+1)} S_h \leq 1,$ then the Picard operator gives a contradiction,

So Eq. (6), (7) solution is unique.

**Disaese Free Equilibrum Point**

Disease free equilibrium is a point where there is no disease in the human population.

At disease free equilibrium $\left(S_h^0 \neq 0, \mathrm{E}_Z^0 = 0, \mathrm{I}_Z^0 = 0, \mathrm{T}_Z^0 = 0, \mathrm{R}_Z^0 = 0, S_V^0 \neq 0, \mathrm{E}_V^0 = 0, \mathrm{I}_V^0 = 0\right).$

$$\left(S_h^0, \mathrm{E}_Z^0, \mathrm{I}_Z^0, \mathrm{T}_Z^0, \mathrm{R}_Z^0, S_V^0, \mathrm{E}_V^0, \mathrm{I}_V^0\right) = \left(\frac{\Lambda_h}{\mu_h}, 0, 0, 0, 0, \frac{\Lambda_V}{\mu_V}, 0, 0\right). \quad (24)$$

**Zika virus Basic Reproduction Number**

The basic reproduction number of Zika virus infected individuals denoted by $R_0^Z$ is defined as the average number of secondary infections produced by introduction of a single Zika virus infectious individual introduced in a wholly susceptible population during his or her entire infectious period. We calculate the basic reproduction number by using the next generation operator method on the dynamical system (1) [23,26].
Hence, it follows that

$R_0^Z = \rho\left(FV^{-1}\right)$ where $\rho$ is the dominant Eigen value of $FV^{-1}$

To find the basic reproduction number $R_0^Z$ for the Zika virus model, we use the formula: $R_0^Z = \rho(FV^{-1})$ where $\rho$ denotes the spectral radius, $F$ is the matrix of new infections, and $V$ is the matrix of transitions.
Given:

$$F = \begin{pmatrix} 0 & \beta_1 & \beta_2 & \beta_3 & 0 \\ 0 & 0 & 0 & 0 & 0 \\ 0 & 0 & 0 & 0 & 0 \\ 0 & \frac{\beta_V \Lambda_V \mu_h}{\Lambda_h \mu_V} & 0 & 0 & 0 \\ 0 & 0 & 0 & 0 & 0 \end{pmatrix} \quad \textbf{and} \quad V = \begin{pmatrix} P_2 & \beta_1 & \beta_2 & \beta_3 & 0 \\ -\alpha & P_3 & 0 & 0 & 0 \\ 0 & -\theta & P_4 & 0 & 0 \\ 0 & \frac{\beta_V \Lambda_V \mu_h}{\Lambda_h \mu_V} & 0 & P_7 & 0 \\ 0 & 0 & 0 & -\theta_V & P_8 \end{pmatrix}.$$

(25)

$$V^{-1}=\begin{pmatrix} \frac{1}{P_2} & 0 & 0 & 0 & 0 \\ \frac{\alpha}{P_3P_2} & \frac{1}{P_3} & 0 & 0 & 0 \\ \frac{\theta\alpha}{P_3P_2P_4} & \frac{\theta}{P_3P_4} & \frac{1}{P_4} & 0 & 0 \\ 0 & 0 & 0 & \frac{1}{P_7} & 0 \\ 0 & 0 & 0 & \frac{\theta_V}{P_7P_8} & \frac{1}{P_8} \end{pmatrix},$$

$$FV^{-1}=\begin{pmatrix} \frac{\beta_1\alpha}{P_2P_3}+\frac{\beta_2\theta\alpha}{P_2P_3P_4} & \frac{\beta_1}{P_3}+\frac{\beta_2\theta}{P_3P_4} & \frac{\beta_2}{P_4} & \frac{\beta_3}{P_7} & 0 \\ 0 & 0 & 0 & 0 & 0 \\ 0 & 0 & 0 & 0 & 0 \\ \frac{\beta_V\Lambda_V\mu_h\alpha}{\Lambda_h\mu_VP_2P_3} & \frac{\beta_V\Lambda_V\mu_h}{\Lambda_h\mu_VP_3} & 0 & 0 & 0 \\ 0 & 0 & 0 & 0 & 0 \end{pmatrix},$$

$$R_0^Z=\frac{1}{2}\left(\frac{\begin{array}{l}\alpha\theta\Lambda_h\left(\theta_V+\mu_h\right)\beta_2\mu_V+\alpha\Lambda_h\left(\sigma+\delta_2+\mu_h\right)\left(\theta_V+\mu_h\right)\beta_1\mu_v \\ +\sqrt{\begin{array}{l}\alpha^2\theta^2{\Lambda_h}^2\left(\theta_V+\mu_h\right)\beta_2{}^2{\mu_V}^2+2\alpha^2\theta{\Lambda_h}^2\left(\sigma+\delta_2+\mu_h\right) \\ \left(\theta_V+\mu_h\right)^2\beta_1\beta_2{\mu_v}^2+\alpha^2{\Lambda_h}^2\left(\sigma+\delta_2+\mu_h\right)^2\left(\theta_V+\mu_h\right)^2\beta_1{}^2{\mu_v}^2 \\ +4\alpha\Lambda_h\Lambda_V\left(\alpha+\mu_h\right)\left(\theta+\delta_1+\mu_h\right)\left(\sigma+\delta_2+\mu_h\right)^2\left(\theta_V+\mu_h\right)\beta_3\beta_V\mu_h\mu_V\end{array}}\end{array}}{\left(\theta+\delta_1+\mu_h\right)\left(\alpha+\mu_h\right)\left(\sigma+\delta_2+\mu_h\right)^2\Lambda_h\mu_V\left(\theta_V+\mu_h\right)}\right),$$

(26)

Where

$$P_1=\mu_h, P_2=\left(\alpha+\mu_h\right), P_3=\left(\theta+\delta_1+\mu_h\right), P_4=\left(\sigma+\delta_2+\mu_h\right),$$
$$P_5=\left(\omega+\mu_h\right), P_6=\mu_V, \mathrm{P}_7=\mu_V, \mathrm{P}_8=\left(\delta_V+\mu_V\right).$$

This implies the dominant Eigen value.

**Zika virus Endemic Equilibrium Point**

Endemic equilibrium point is a steady where the diseases persist in the human population.

At endemic equilibrium point [23,24]

$\left(S_h^* \neq 0, \mathrm{E}_Z^* \neq 0, \mathrm{I}_Z^* \neq 0, \mathrm{T}_Z^* \neq 0, \mathrm{R}_Z^* \neq 0, S_V^* \neq 0, \mathrm{E}_V^* \neq 0, \mathrm{I}_V^* \neq 0\right).$

$$S_h^* = -\frac{\Lambda_h P_2 P_3 P_4 P_5}{-P_2 P_3 P_4 P_5 \left(\lambda_h + P_1\right) + \alpha\omega\sigma\theta\lambda_h},$$

$$E_Z^* = -\frac{\Lambda_h P_3 P_4 P_5 \lambda_h}{\alpha\omega\sigma\theta\lambda_h - P_2 P_3 P_4 P_5 P_1 - P_2 P_3 P_4 P_5 \lambda_h},$$

$$I_Z^* = -\frac{\alpha\Lambda_h P_4 P_5 \lambda_h}{\alpha\omega\sigma\theta\lambda_h - P_2 P_3 P_4 P_5 P_1 - P_2 P_3 P_4 P_5 \lambda_h},$$

$$T_Z^* = -\frac{\alpha\Lambda_h P_5 \lambda_h \theta}{\alpha\omega\sigma\theta\lambda_h - P_2 P_3 P_4 P_5 P_1 - P_2 P_3 P_4 P_5 \lambda_h}, \tag{27}$$

$$R_Z^* = -\frac{\sigma\alpha\Lambda_h \lambda_h \theta}{\alpha\omega\sigma\theta\lambda_h - P_2 P_3 P_4 P_5 P_1 - P_2 P_3 P_4 P_5 \lambda_h},$$

$$S_V^* = \frac{\Lambda_V \left(\alpha\sigma\theta\lambda_h + \alpha\theta P_5 \lambda_h + \alpha P_4 P_5 \lambda_h + P_2 P_3 P_4 P_5 + P_3 P_4 P_5 \lambda_h\right)}{\alpha\sigma\theta P_6 \lambda_h + \alpha\theta P_5 P_6 \lambda_h + \alpha P_4 P_5 P_6 \lambda_h + \alpha P_4 P_5 \beta_V \lambda_h + P_2 P_3 P_4 P_5 P_6 + P_3 P_4 P_5 P_6 \lambda_h},$$

$$E_V^* = \frac{P_4 P_5 \beta_V \lambda_h \alpha \Lambda_V}{P_7 \left(\alpha\sigma\theta P_6 \lambda_h + \alpha\theta P_5 P_6 \lambda_h + \alpha P_4 P_5 P_6 \lambda_h + \alpha P_4 P_5 \beta_V \lambda_h + P_2 P_3 P_4 P_5 P_6 + P_3 P_4 P_5 P_6 \lambda_h\right)},$$

$$I_V^* = -\frac{\theta_V \lambda_h P_3 P_4 P_5 \Lambda_h}{\left(\alpha\omega\sigma\theta\lambda_h - P_2 P_3 P_4 P_5 P_1 - P_2 P_3 P_4 P_5 \lambda_h\right) P_8}.$$

Substituting into the force of infections: $\lambda_h = \frac{\left(\beta_1 I_Z + \beta_2 T_Z + \beta_3 I_V\right)}{N_h}$ and $\lambda_V = \frac{\beta_V I_Z}{N_h}$.

We have:

$$Q_1 = \left(\alpha\sigma\theta P_8 + \alpha\theta P_5 P_8 + \alpha P_4 P_5 P_8 + P_3 P_4 P_5 P_8\right),$$

$$Q_2 = \left(-\alpha\theta P_5 P_8 \beta_2 - \alpha P_4 P_5 P_8 \beta_1 + P_2 P_3 P_4 P_5 P_8 - P_3 P_4 P_5 \beta_3 \theta_V\right)$$

$$Q_2 = P_2 P_3 P_4 P_5 P_8 \left(1 - \left(R_0^Z\right)^2\right). \tag{28}$$

if $R_0^Z < 1$.

The endemic equilibrium points are obtained from solving for $\lambda_Z^{**}$ in the polynomial, and substituting the positive values of $\lambda_Z^{**}$ into the expression *, Furthermore, it

follows that the coefficient is always positive, and is positive (negative) if $R_0^Z$ is less (greater) than one.

**Zika virus Sensitivity Analysis**

Sensitivity analysis is performed to determine the sensitive parameters that influence the spread of Zika virus in the human population [24,25] .

It can be calculated using the formula:

$$S_\theta^{R_0^Z} = \left(\frac{\partial R_0^Z}{\partial \theta}\right)\left(\frac{R_0^Z}{\theta}\right).$$

$$S_\theta^{R_0^Z} = 0.56254, S_{\theta_V}^{R_0^Z} = 0.3528, S_{\Lambda_h}^{R_0^Z} = 0.0049, S_\alpha^{R_0^Z} = 0.6258, S_{\mu_h}^{R_0^Z} = -0.00785,$$
$$S_\sigma^{R_0^Z} = -0.8321, S_{\delta_1}^{R_0^Z} = -0.0425, S_{\delta_2}^{R_0^Z} = -0.023, S_{\beta_3}^{R_0^Z} = 0.4721, S_{\beta_V}^{R_0^Z} = 0.5927,$$
$$S_{\beta_1}^{R_0^Z} = 0.5631, S_{\beta_2}^{R_0^Z} = 0.036, S_{\mu_V}^{R_0^Z} = -0.00521.$$

(29)

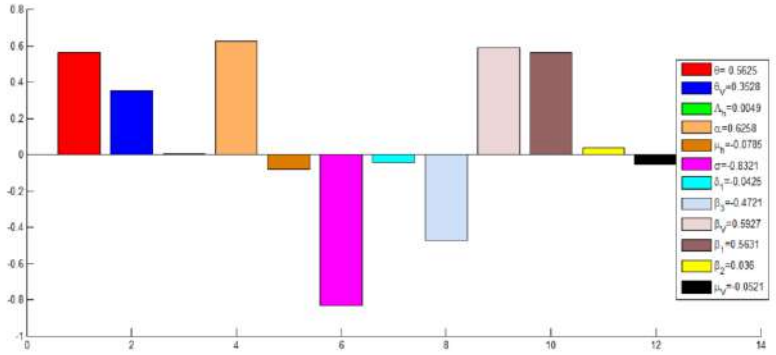


Figure. 2: Zika Virus sensitivity Bar chart

**Fractional order model numerical results**

The same fractional-order Zika virus model was numerically solved by using the generalized fractional Adams-Bashforth-Moulton technique [23,26]. Table 1 showed the parameters values of the model and Table 2 shows the different fractional values of the order used and simulated in the model.

$${}^cD_t^\psi P(t) = Q(t, \mathrm{q}(t)),\ 0 < t < \beta, \qquad (30)$$

$$P^{(n)}(0) = P_0^{(n)},\ n = 1, 0, ..., \mathrm{q}, \mathrm{q} = [\alpha].$$

The $P=\left(S_h^*,\mathrm{E}_Z^*,\mathrm{I}_Z^*,\mathrm{T}_Z^*,\mathrm{R}_Z^*,\mathrm{S}_V^*,\mathrm{E}_V^*,\mathrm{I}_V^*\right)\in R_+^8$ and $V\left(t,\mathrm{q}\left(t\right)\right)$ is a continuous function of a real value. the above fractional order can hence be expressed in terms of the idea of fractional integral as follows:

$$P\left(t\right)=\sum_{n=0}^{m-1}P_0^{(n)}\frac{t^n}{n!}+\frac{1}{\Gamma\left(\psi\right)}\int_0^t\left(t-y\right)^{\psi-1}R\left(\mathrm{k},m\left(k\right)\right)dk \tag{31}$$

Using the method described in [23,24] , we let the step size $g=\frac{\beta}{N}$, $N\in\mathrm{N}$ with a grid that is uniform on $\left[0,\beta\right]$. Where $t_c=cr$, $c=0,1,1,...N$. Thus, and fractional order model of Zika virus model could be well approximated as (7) creates:

$$S_{h(k+1)}\left(t\right)=S_{h0}+\frac{g^\psi}{\Gamma\left(\psi+2\right)}\left\{\Lambda_h+\omega R_Z^n-\frac{\left(\beta_1I_Z^n+\beta_2T_Z^n+\beta_3I_V^n\right)}{N_h^n}S_h^n-\mu_hS_h^n\right\}+$$

$$\frac{g^\psi}{\Gamma\left(\psi+2\right)}\sum_{y=0}^{k}dy,k+1\left\{\Lambda_h+\omega R_{Zy}-\frac{\left(\beta_1I_{Zy}+\beta_2T_{Zy}+\beta_3I_{Vy}\right)}{N_{hy}}S_{hy}-\mu_hS_{hy}\right\},$$

$$E_{Z(k+1)}\left(t\right)=E_{Z0}+\frac{g^\psi}{\Gamma\left(\psi+2\right)}\left\{\frac{\left(\beta_1I_Z^n+\beta_2T_Z^n+\beta_3I_V^n\right)}{N_h^n}S_h^n-\left(\alpha+\mu_h\right)E_Z^n\right\}+$$

$$\frac{g^\psi}{\Gamma\left(\psi+2\right)}\sum_{y=0}^{k}dy,k+1\left\{\frac{\left(\beta_1I_{Zy}+\beta_2T_{Zy}+\beta_3I_{Vy}\right)}{N_{hy}}S_{hy}-\left(\alpha+\mu_h\right)E_{Zy}\right\},$$

(32)

$$I_{Z(k+1)}\left(t\right)=I_{Z0}+\frac{g^\psi}{\Gamma\left(\psi+2\right)}\left\{\alpha E_Z^n-\left(\theta+\delta_1+\mu_h\right)I_Z^n\right\}+$$

$$\frac{g^\psi}{\Gamma\left(\psi+2\right)}\sum_{y=0}^{k}dy,k+1\left\{\alpha E_{Zy}-\left(\theta+\delta_1+\mu_h\right)I_{Zy}\right\},$$

$$T_{Z(k+1)}\left(t\right)=T_{Z0}+\frac{g^\psi}{\Gamma\left(\psi+2\right)}\left\{\theta I_Z^n-\left(\sigma+\delta_2+\mu_h\right)T_Z^n\right\}+$$

$$\frac{g^\psi}{\Gamma\left(\psi+2\right)}\sum_{y=0}^{k}dy,k+1\left\{\theta I_{Zy}-\left(\sigma+\delta_2+\mu_h\right)T_{Zy}\right\},$$

$$R_{Z(k+1)}\left(t\right)=R_{Z0}+\frac{g^\psi}{\Gamma\left(\psi+2\right)}\left\{\sigma T_Z^n-\left(\omega+\mu_h\right)R_Z^n\right\}+$$

$$\frac{g^\psi}{\Gamma\left(\psi+2\right)}\sum_{y=0}^{k}dy,k+1\left\{\sigma T_{Zy}-\left(\omega+\mu_h\right)R_{Zy}\right\},$$

$$S_{V(k+1)}(t)=S_{V0}+\frac{g^{\psi}}{\Gamma(\psi+2)}\left\{\Lambda_V-\frac{\beta_V I_Z^n}{N_h}S_V^n-\mu_V S_V^n\right\}+$$
$$\frac{g^{\psi}}{\Gamma(\psi+2)}\sum_{y=0}^{k}dy,k+1\left\{\Lambda_V-\frac{\beta_V I_{Zy}}{N_{hy}}S_{Vy}-\mu_V S_{Vy}\right\},$$

$$E_{V(k+1)}(t)=E_{V0}+\frac{g^{\psi}}{\Gamma(\psi+2)}\left\{\frac{\beta_V I_Z^n}{N_h^n}S_V^n-(\theta_V+\mu_V)E_V^n\right\}+$$
$$\frac{g^{\psi}}{\Gamma(\psi+2)}\sum_{y=0}^{k}dy,k+1\left\{\frac{\beta_V I_{Zy}}{N_{hy}}S_V-(\theta_V+\mu_V)E_V\right\},$$

$$I_{V(k+1)}(t)=I_{V0}+\frac{g^{\psi}}{\Gamma(\psi+2)}\left\{\theta_V E_V^n-(\delta_V+\mu_V)I_V^n\right\}+$$
$$\frac{g^{\psi}}{\Gamma(\psi+2)}\sum_{y=0}^{k}dy,k+1\left\{\theta_V E_{Vy}-(\delta_V+\mu_V)I_{Vy}\right\}.$$

Where

$$S_{h(k+1)}^n(t)=S_{h0}+\frac{1}{\Gamma(\psi)}\sum_{y=0}^{k}f_{y,k+1}\left\{\Lambda_h+\omega R_{Zy}-\frac{(\beta_1 I_{Zy}+\beta_2 T_{Zy}+\beta_3 I_{Vy})}{N_{hy}}S_{hy}-\mu_h S_{hy}\right\},$$

$$E_{Z(k+1)}^n(t)=E_{Z0}+\frac{1}{\Gamma(\psi)}\sum_{y=0}^{k}f_{y,k+1}\left\{\frac{(\beta_1 I_{Zy}+\beta_2 T_{Zy}+\beta_3 I_{Vy})}{N_{hy}}S_{hy}-(\alpha+\mu_h)E_{Zy}\right\},$$

(33)

$$I_{Z(k+1)}^n(t)=I_0+\frac{1}{\Gamma(\psi)}\sum_{y=0}^{k}f_{y,k+1}\left\{\alpha E_{Zy}-(\theta+\delta_1+\mu_h)I_{Zy}\right\},$$

$$T_{Z(k+1)}^n(t)=I_0+\frac{1}{\Gamma(\psi)}\sum_{y=0}^{k}f_{y,k+1}\left\{\theta I_{Zy}-(\sigma+\delta_2+\mu_h)T_{Zy}\right\},$$

$$R_{Z(k+1)}^n(t)=I_0+\frac{1}{\Gamma(\psi)}\sum_{y=0}^{k}f_{y,k+1}\left\{\sigma T_{Zy}-(\omega+\mu_h)R_{Zy}\right\},$$

$$S_{V(k+1)}^n(t)=I_0+\frac{1}{\Gamma(\psi)}\sum_{y=0}^{k}f_{y,k+1}\left\{\Lambda_V-\frac{\beta_V I_{Zy}}{N_{hy}}S_{Vy}-\mu_V S_{Vy}\right\},$$

$$E_{V(k+1)}^n(t)=I_0+\frac{1}{\Gamma(\psi)}\sum_{y=0}^{k}f_{y,k+1}\left\{\frac{\beta_V I_{Zy}}{N_{hy}}S_V-(\theta_V+\mu_V)E_V\right\},$$

$$I^{n}_{V(k+1)}(t) = I_0 + \frac{1}{\Gamma(\psi)}\sum_{y=0}^{k} f_{y,k+1}\left\{\theta_V E_{Vy} - (\delta_V + \mu_V) I_{Vy}\right\}.$$

From (4.29) and (4.30) obtained;

$$dy,_{K+1} = K^{\psi+1} - (k-\psi)(k+\psi)^{\psi},\ y = 0.$$

$$(k-y+2)^{\psi+1} + (k-\psi)^{\psi+1} - 2(k-y+1)^{\psi+1},\ 1 \le y \le k$$

and $f_{y,k+1} = \frac{g^{\psi}}{\psi}\left[(k-y+1)^{\psi}(k-y)^{\psi}\right],\ 0 \le y \le k.$

**Numerical Simulation and Results**

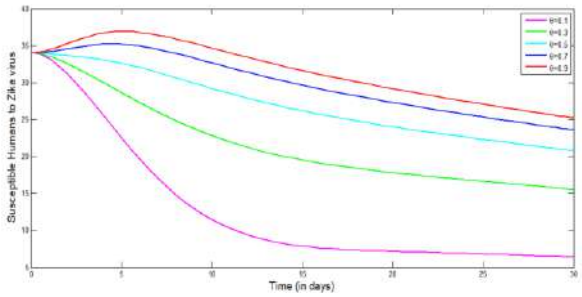


Figure 3a: Simulation of the effect of $(\theta)$ on susceptible human population

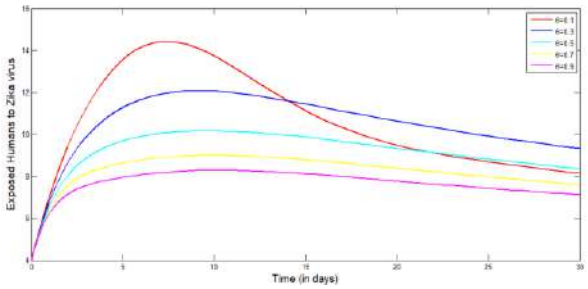


Figure 3b: Simulation of the effect of $(\theta)$ on Exposed human population

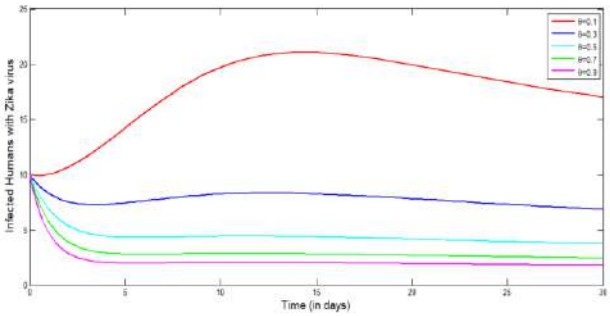


Figure 4a: Simulation of the effect of $(\theta)$ on Infected human population

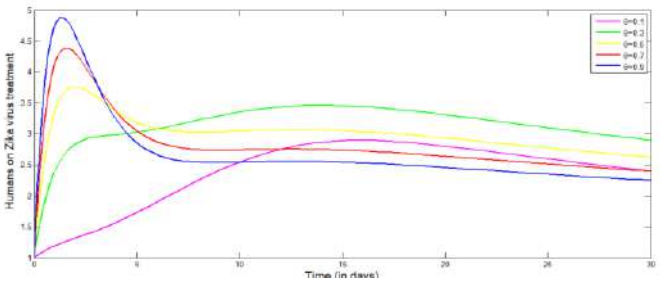


Figure 4b: Simulation of the effect of $(\theta)$ on human population on treatment

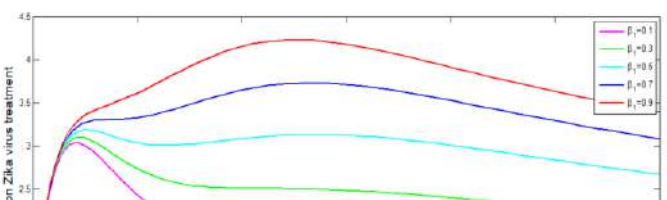

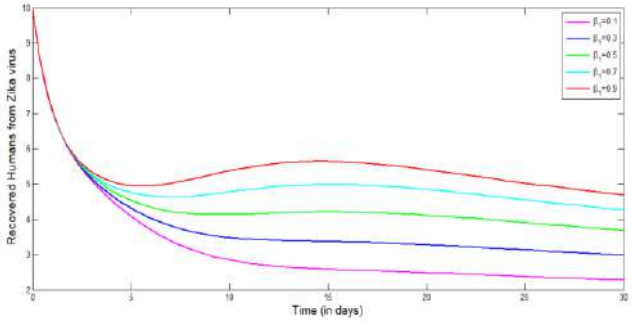


Figure 5a: Simulation of the effect of $(\beta_1)$ on human population on treatment

Figure 5b: Simulation of the effect of $(\beta_1)$ on Recovered human population

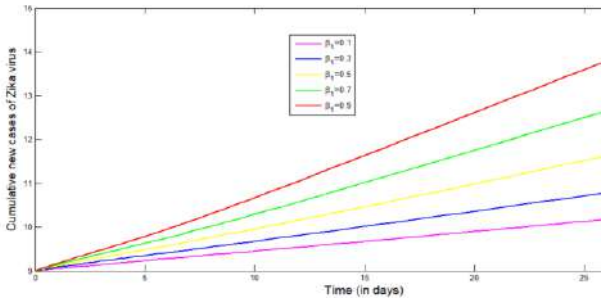


Figure 6a: Simulation of the effect of $(\beta_1)$ on Cumulative new cases of Zika virus

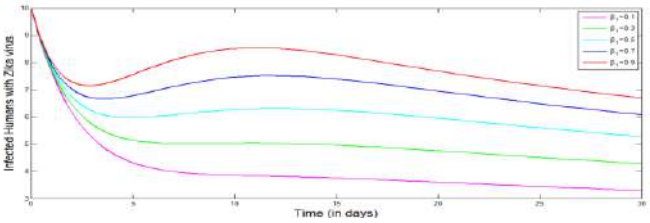


Figure 6b: Simulation of the effect of $(\beta_1)$ on infected human population

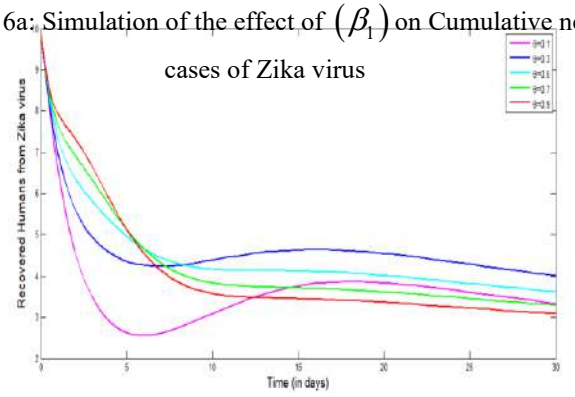


Figure 7a: Simulation of the effect of $(\theta)$ on Recovered human population

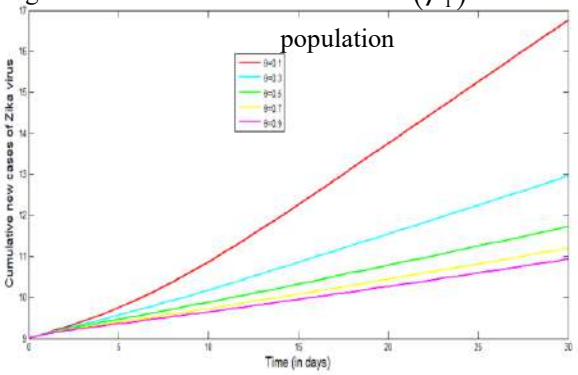


Figure 7b: Simulation of the effect of $(\theta)$ on Cumulative new cases of Zika virus

**Table 2.** Parameter Values used for the Zika Virus model simulations

| Parameter | Typical Value / Range | Sources |
|---|---|---|
| $\Lambda_h$ | 0.29 | [17] |
| $\mu_h$ | 0.056 | [17] |
| $\alpha$ | 0.182 | [24] |
| $\theta$ | 0.05 | [17] |
| $\sigma$ | 0.167 | Assumed |
| $\omega$ | 0.01 | Assumed |
| $\delta_1$ | 0.001 | [25] |

| | | |
|---|---|---|
| $\delta_2$ | 0.0005 | [19] |
| $\Lambda_V$ | 0.05 | Assumed |
| $\mu_V$ | 0.071 | [20] |
| $\theta_V$ | 0.122 | [20] |
| $\delta_V$ | 0.004 | [21] |
| $\beta_V$ | 0.7 | [19] |
| B | 0.3 | Assumed |

**Figure 2a,** the susceptible population decreases over time for all values of θ, but the rate of decline depends on the magnitude of θ. When θ is small, the susceptible population declines more sharply, meaning that more individuals are getting infected due to lower treatment levels. As θ increases, the decline becomes more gradual, and the susceptible curve remains higher throughout the simulation. This indicates that higher treatment rates effectively reduce infection spread, thereby protecting more individuals from becoming exposed or infected. The highest curve (θ = 0.9) shows that a large proportion of the population remains susceptible because the enhanced treatment reduces transmission significantly. In **Figure 2b**, the exposed population initially increases with time and then decreases after reaching a peak. This behavior is typical of epidemic dynamics, where exposure rises as new infections occur and later falls as individuals progress to infection or recovery. For smaller θ values, the exposed class rises sharply and reaches a higher peak, reflecting rapid disease transmission under low treatment conditions. As θ increases, the exposed population peak becomes lower and occurs earlier, showing that treatment reduces the number of individuals who progress from susceptible to exposed. When θ is highest (θ = 0.9), the exposed curve remains the lowest throughout, confirming that increased treatment effectively curtails the rate at which people become exposed to the virus. Both figures demonstrate that increasing the treatment rate (θ) suppresses the spread of Zika virus by maintaining a larger susceptible population and reducing the exposed population. This means treatment plays a crucial role in limiting disease transmission and controlling epidemic intensity. In **Figure 4a**, which represents the infected human population, all the curves begin at a similar point but show distinct trends depending on the value of θ. For smaller θ values, such as θ = 0.1, the infected population rises sharply to a high peak before gradually declining. This indicates that when treatment is less effective or less available, infections spread rapidly, leading to a larger number of infected individuals. As θ increases, the infection curve flattens, and the peak becomes lower and occurs earlier. For higher values of θ (e.g., θ = 0.9), the infected population remains consistently low throughout the simulation period. This trend demonstrates that higher treatment rates significantly reduce the number of infected individuals by hastening recovery and preventing further transmission. Overall, increasing θ suppresses infection prevalence and accelerates the decline of active cases. In **Figure 4b**, which shows the population of humans receiving treatment, the curves display an opposite pattern. When θ is low, the number of individuals on treatment remains small and declines quickly, reflecting insufficient treatment intervention. As θ increases, the treatment population rises to a higher peak and stabilizes at a larger value over time. The highest treatment rate (θ = 0.9) yields the largest population under treatment, indicating that more infected individuals are being identified and managed effectively. The initial peaks in the treatment curves correspond to the early phase of the outbreak when infection is spreading rapidly, followed by a gradual adjustment as treatment balances disease progression and recovery. Together, these graphs reveal that increasing the treatment rate (θ) leads to a decline

in infection levels (Figure 4a) and a corresponding increase in the number of individuals receiving treatment (Figure 4b). This shows that effective treatment not only reduces disease burden but also enhances overall control of Zika virus transmission within the human population. In **Figure 5a**, which shows the effect of $\beta_1$ on the human population under treatment, all curves initially rise as treatment begins to take effect. However, the peak level and trend of the curves depend strongly on $\beta_1$. When $\beta_1$ is low ($\beta_1 = 0.1$), the number of humans on treatment remains small and stable, indicating that fewer infections are occurring, so fewer individuals require treatment. As $\beta_1$ increases, the treatment population rises sharply, reaching higher peaks and maintaining higher levels throughout the simulation. This happens because a higher contact rate increases the number of new infections, thereby enlarging the pool of individuals who need treatment. For $\beta_1 = 0.9$, the highest curve is observed, showing that intense transmission leads to greater treatment demand. The figure indicates that as the contact rate increases, the number of people receiving treatment also increases due to elevated infection pressure. In **Figure 5b**, which displays the effect of $\beta_1$ on the recovered human population, the opposite trend is seen. At lower $\beta_1$ values, the recovered population remains relatively high and stable because fewer people are becoming infected, and recovery proceeds efficiently. As $\beta_1$ increases, the recovered population declines progressively, indicating that high transmission rates reduce the proportion of individuals who can recover within the observed period. This decline is due to continuous new infections overwhelming recovery efforts or prolonging the infectious period. The curves also show that at higher $\beta_1$ values, recovery occurs more slowly and stabilizes at lower levels, reflecting a heavier disease burden in the population.

These two figures demonstrate that an increase in the contact rate ($\beta_1$) intensifies disease transmission, leading to more individuals requiring treatment (Figure 5a) but fewer achieving full recovery (Figure 5b)**.** This highlights that reducing contact between susceptible and infectious individuals through public health measures like vector control, personal protection, or social interventions is crucial for minimizing infection spread and improving recovery outcomes in the human population. In **Figure 6a,** which illustrates the effect of $\beta_1$ on the cumulative new cases of Zika virus, all the curves show an upward trend over time, reflecting the continuous accumulation of new infections. However, the slope of the curves varies with the value of $\beta_1$. When $\beta_1$ is low ($\beta_1 = 0.1$), the curve rises slowly, meaning that fewer individuals are becoming infected over time due to limited contact and slower transmission. As $\beta_1$ increases, the cumulative cases grow much faster, with the steepest rise occurring for $\beta_1 = 0.9$. This implies that a higher contact rate causes rapid and sustained growth in the number of new infections. The consistent separation between the curves demonstrates a direct positive relationship between $\beta_1$ and disease spread the higher the contact rate, the greater the cumulative burden of infection within the human population. In **Figure 6b,** which shows the effect of $\beta_1$ on the infected human population**,** all the curves initially decline and then rise to varying degrees before stabilizing. At lower $\beta_1$ values, such as $\beta_1 = 0.1$, the infected population remains low, indicating that transmission is weak and new infections are quickly contained. As $\beta_1$ increases, the infected population becomes larger and stabilizes at higher levels, with $\beta_1 = 0.9$ producing the highest curve. This pattern shows that higher contact rates sustain a larger pool of infectious individuals by increasing the number of susceptible people becoming infected and slowing down recovery relative to infection spread. The peaks of the curves also occur earlier at higher $\beta_1$ values, indicating that outbreaks progress faster when transmission is more intense. These two figures clearly show that increasing the contact rate ($\beta_1$) accelerates the spread of the Zika virus by raising the number of new infections (Figure 6a) and increasing the proportion of the population that remains infected at any time (Figure 6b)**.** This demonstrates

that controlling human vector contact through measures such as vector control, repellents, and public health awareness is critical for reducing transmission and preventing large outbreaks of the Zika virus. In **Figure 7a**, which shows the effect of θ on the recovered human population**,** all the curves begin at similar values but diverge as time progresses. For smaller θ values (e.g., θ = 0.1), the recovered population declines sharply and remains low, indicating that fewer individuals are being successfully treated and moved into the recovery class. As θ increases, the decline becomes slower, and the recovered population stabilizes at higher values. This means that higher treatment rates accelerate recovery and reduce the duration of infection, leading to a larger number of recovered individuals over time. The highest recovery curve corresponds to θ = 0.9, showing that intensive treatment interventions can effectively raise the recovery level within the population. The early dip in all curves represents the initial infection surge, after which treatment begins to take effect, gradually increasing the number of people recovering from the disease. In **Figure 7b,** which depicts the effect of θ on the cumulative new cases of Zika virus, the curves increase steadily over time, showing that new infections continue to occur throughout the simulation period. However, the rate of increase depends on the value of θ. When θ is small (θ = 0.1), the cumulative cases rise very quickly, leading to the steepest curve indicating that low treatment coverage allows infection to spread rapidly. As θ increases, the slope of the curve decreases, showing that higher treatment rates slow down the accumulation of new cases. For θ = 0.9, the curve rises very gradually, meaning that only a small number of new infections occur when treatment is widely available and effective. The two figures demonstrate opposite but complementary effects of the treatment rate. Increasing θ enhances recovery (Figure 7a) while simultaneously reducing the total number of new infections (Figure 4.10). This clearly indicates that effective and timely treatment plays a vital role in curbing the spread of the Zika virus**,** decreasing infection incidence, and improving recovery outcomes within the human population.

## Conclusion

This study investigated the impact of treatment rate and contact rate on the transmission dynamics of the Zika virus using a deterministic compartmental model. The analysis of the basic reproduction number ( $R_0^Z$ ) revealed its crucial role as a threshold parameter determining whether the infection will persist or die out in the population. Simulation results showed that an increase in the contact rate ($\beta_1$) leads to a significant rise in the number of infected humans and cumulative new cases, thereby increasing the reproduction number and sustaining disease transmission. Conversely, an increase in the treatment rate ( $R_0^Z$ ) results in a reduction in the infected population and new infections, while enhancing the number of recovered individuals. The contour and surface plots further demonstrated that $R_0^Z$ decreases with an increase in the treatment rate and increases with higher contact rates. When the treatment rate is sufficiently high, $R_0^Z$ falls below unity, leading to the eventual elimination of the disease from the population. These findings highlight that treatment intervention plays a vital role in controlling and possibly eradicating Zika virus infection, especially in populations with high contact intensity. The results confirm that the interplay between treatment rate and contact rate strongly influences the progression and control of Zika virus spread. Effective treatment coverage, coupled with reduced contact between susceptible and infected individuals can drive the infection toward extinction and restore population health stability.

Based on the findings of this study, the following recommendations were made:

1. Public health authorities should strengthen treatment interventions for infected individuals to increase recovery rates and reduce the infectious period, thereby lowering the basic reproduction number ( $R_0^Z$ ).
2. Strategies such as vector control, use of mosquito repellents, and community sensitization campaigns should be intensified to minimize human–vector contact and prevent new infections.
3. Combining treatment with preventive strategies such as vaccination (where available), improved sanitation, and environmental management will provide a more sustainable reduction in transmission.
4. Continuous public awareness campaigns should be carried out to educate communities about preventive behaviors and the importance of early treatment to curb disease spread.
5. Governments and research institutions should invest in data-driven modeling studies to guide policy decisions and assess the long-term effectiveness of various intervention strategies under different epidemiological settings.

## References

[1] Mlakar, J., Korva, M., Tul, N., Popović, M., Poljšak-Prijatelj, M., Mraz, J., Kolenc, M., Resman Rus, K., Vesnaver Vipotnik, T., Fabjan Vodušek, V., Vizjak, A., Pižem, J., Petrovec, M., & Avšič Županc, T. (2016). Zika virus associated with microcephaly. *New England Journal of Medicine, 374*(10), 951–958. Zika virus associated with microcephaly

[2] Johansson, M. A., Mier-y-Teran-Romero, L., Reefhuis, J., Gilboa, S. M., & Hills, S. L. (2016). Zika and the risk of microcephaly. *New England Journal of Medicine, 375*(1), 1–4. Zika and the risk of microcephaly

[3] Petersen, L. R., Jamieson, D. J., Powers, A. M., & Honein, M. A. (2016). Zika virus. *New England Journal of Medicine, 374*(16), 1552–1563. Zika virus overview NEJM

[4] Musso, D., & Gubler, D. J. (2016). Zika virus. *Clinical Microbiology Reviews, 29*(3), 487–524. Zika virus Clinical Microbiology Reviews

[5] Broutet, N., Krauer, F., Riesen, M., Khalakdina, A., Almiron, M., Aldighieri, S., Espinal, M., Low, N., & Dye, C. (2016). Zika virus as a cause of neurologic disorders. *New England Journal of Medicine, 374*(16), 1506–1509. Zika virus neurologic disorders NEJM

[6] Brasil, P., Pereira, J. P., Moreira, M. E., Ribeiro Nogueira, R. M., Damasceno, L., Wakimoto, M., Rabello, R. S., Valderramos, S. G., Halai, U. A., Salles, T. S., Zin, A. A., Horovitz, D., Daltro, P., Boechat, M., Raja Gabaglia, C., Carvalho de Sequeira, P., Pilotto, J. H., Medialdea-Carrera, R., Cotrim da Cunha, D., & Nielsen-Saines, K. (2016). Zika virus infection in pregnant women in Rio de Janeiro. *New England Journal of Medicine, 375*(24), 2321–2334. Zika infection in pregnancy Rio study

[7] Gongora-Rivera, F., Grijalva, I., Infante-Valenzuela, A., Cámara-Lemarroy, C., Garza- González, E., Paredes-Cruz, M., Grajales-Muñiz, C., Guerrero-Cantera, J., Vargas-Ramos, I., & Soares, J. (2020). Zika virus infection and Guillain-Barré syndrome in Northeastern Mexico: A case-control study. *PLOS ONE, 15*(3), e0230132. Zika Guillain Barre case control study (PLOS)

[8] Clemente, N. S., Brickley, E. B., Paixão, E. S., de Almeida, M. F., Gazeta, R. E., Vedovello, D., Rodrigues, L. C., Witkin, S. S., & Passos, S. D. (2020). Zika virus infection in pregnancy and adverse fetal outcomes in São Paulo State, Brazil: A prospective cohort study. *Scientific Reports, 10*, 12673. Zika pregnancy cohort Brazil study (Nature)

[9] Silva, P. F. S., Eickmann, S. H., Ximenes, R. A. A., Montarroyos, U. R., Lima, M. C., Martelli, C. M. T., Barreto de Araújo, T. V., Brickley, E. B., Rodrigues, L. C., Gonçalves, F. C. L. S. P., Carvalho, M. D. C. G., Souza, W. V., & Miranda-Filho, D. B. (2020). Pediatric neurodevelopment by prenatal Zika virus exposure: A cross-sectional study. *BMC Pediatrics, 20*, 472.Prenatal Zika neurodevelopment study (Springer Link)

[10] Grant, R., Fléchelles, O., Tressières, B., Elenga, N., Medialdea-Carrera, R., Gaete, S., Hébert, J. C., Schaub, B., Djossou, F., & Hoen, B. (2021). In utero Zika virus exposure and neurodevelopment at 24 months in toddlers normocephalic at birth: A cohort study. *BMC Medicine, 19*, 12.Zika neurodevelopment cohort study 24 months (Springer Link)

[12] Grant, R., Fléchelles, O., Elenga, N., Tressières, B., Gaete, S., Hébert, J. C., Schaub, B., Djossou, F., Mallard, A., & Hoen, B. (2022). Consequences of in utero Zika virus exposure and adverse pregnancy and early childhood outcomes: A prospective cohort study. *Viruses, 14*(12), 2755.Zika pregnancy outcomes cohort Viruses journal (MDPI)

[13] Shaibu, J. O., Akinyemi, K. O., Uzor, O. H., Audu, R. A., & Oyefolu, A. B. O. (2023). Molecular surveillance of arboviruses in Nigeria. *BMC Infectious Diseases, 23*, 538. Molecular surveillance arboviruses Nigeria (Springer Link)

[14] Mac, P. A., Airiohuodion, P. E., Velayudhan, R., Zubair, S., Tadele, M., Aighobahi, J. O., Anyaike, C., Kroeger, A., & Panning, M. (2023). Antibody seropositivity and endemicity of chikungunya and Zika viruses in Nigeria. *Animal Diseases, 3*, 7. Zika seropositivity Nigeria study (SpringerLink)

[15] Khongwichit, S., Chuchaona, W., Vongpunsawad, S., Theamboonlers, A., & Poovorawan, Y. (2023). Molecular epidemiology, clinical analysis, and genetic characterization of Zika virus infections in Thailand (2020–2023). *Scientific Reports, 13*, 21030. Zika epidemiology Thailand 2023 study (Nature)

[16] Teoh, B. T., Chin, K. L., Samsudin, N. I., Loong, S. K., Sam, S. S., & Tan, K. K. (2020). A reverse transcription loop-mediated isothermal amplification for broad coverage detection of Asian and African Zika virus lineages. *BMC Infectious Diseases, 20*, 947. Zika detection RT-LAMP study (Springer Link)

[17] Biswas, S. K., Ghosh, U., & Sarkar, S. (2020). Mathematical model of Zika virus dynamics with vector control and sensitivity analysis. *Infectious Disease Modelling, 5*, 23–41. https://doi.org/10.1016/j.idm.2019.12.001

18] Murugappan, M., Kumar, G. M., Rajchakit, G., & Vetrivel, G. (2023). Mathematical modelling on the transmission dynamics of Zika virus. *International Journal on Robotics, Automation and Sciences, 5*(2). https://doi.org/10.33093/ijoras.2023.5.2.9

[19] Ibrahim, M. A., & Dénes, A. (2023). A mathematical model for Zika virus infection and microcephaly risk considering sexual and vertical transmission. *Axioms, 12*(3), 263. https://doi.org/10.3390/axioms12030263 (Direct link: MDPI article)

[20] Wang, L., Jia, Q., Zhu, G., Ou, G., & Tang, T. (2024). Transmission dynamics of Zika virus with multiple infection routes and a case study in Brazil. *Scientific Reports, 14*, 7424. https://doi.org/10.1038/s41598-024-58025-7

[21] Zhu, J., Khan, F., Khan, S. U., Sumelka, W., Khan, F. U., & AlQahtani, S. A. (2024). Computational investigation of stochastic Zika virus optimal control model using Legendre spectral method. *Scientific Reports, 14*, 18112. https://doi.org/10.1038/s41598-024-69096-x

[22] Derakhshan, M., & Aminataei, A. (2021). *New approach for the chaotic dynamical systems involving Caputo-Prabhakar fractional derivative using Adams-Bashforth scheme*. *Journal of Difference Equations and Applications, 29*(6), 640–656. https://doi.org/10.1080/10236198.2021.1976770 (Taylor & Francis Online)

[23] Babanezhad, M., Behroyan, I., Nakhjiri, A. T., Marjani, A., & Shirazian, S. (2020). *Simulation of liquid flow with a combination artificial intelligence flow field and Adams–Bashforth method*. *Scientific Reports, 10*, 16719. https://doi.org/10.1038/s41598-020-72602-6

[24] Agbata, B. C., Shior, M. M., Obeng-Denteh, W., Omotehinwa, T. O., Paul, R. V., Kwabi, P. A., & Asante-Mensa, F. (2023). *A mathematical model of COVID-19 transmission dynamics with effects of awareness and vaccination program*.

Journal of Ghana Science Association, 21(2), 59–61. https://doi.org/10.5281/zenodo.13954532

[25] Acheneje, G. O., Omale, D., Agbata, B. C., Atokolo, W., Shior, M. M., & Bolarinwa, B. (2024). *Approximate solution of the fractional order mathematical model on the transmission dynamics of the co-infection of COVID-19 and Monkeypox using the Laplace–Adomian decomposition method*. International Journal of Mathematics and Statistics Studies, 12(3), 17–51. https://doi.org/10.37745/ijmss.13/vol12n31751

[26] Ibrahim, S. (2023). *Solution of first-order differential equation using fourth-order Runge-Kutta approach and Adams Bashforth methods*. *International Journal on Recent and Innovation Trends in Computing and Communication, 11*(11), 308–316. https://doi.org/10.17762/ijritcc.v11i11.9504 (IJRITCC)